CHEMISTRY OF MATERIALS

Communication

pubs.acs.org/cm

Reversible Electrochemical Intercalation of Aluminum in Mo_6S_8

Linxiao Geng,[†] Guocheng Lv,[§] Xuebing Xing,[§] and Juchen Guo*[,†,‡]

[†]Department of Chemical and Environmental Engineering and [‡]Materials Science and Engineering Program, University of California, Riverside, Riverside, California 92521, United States

[§]School of Materials Sciences and Technology, China University of Geosciences, Beijing, Beijing 100083, China

Supporting Information

Among the rechargeable batteries beyond lithium chemistry, the ones based on aluminum (Al) are particularly promising: Al not only is the most abundant metal in the earth's crust but also has attractive capacity due to its trivalency. To date, there were only scarce investigations on rechargeable Al batteries in literature. The initial investigations, as summarized in the review article by Li and Bjerrum,[1] were focused on identifying Al-ion electrolytes from organic solvents and demonstrating potential cathode materials. However, these early attempts had little success due to the sluggish electrochemical Al deposition−dissolution in organic solvents.[2−4] On the other hand, reversible electrochemical Al deposition−dissolution could be facilely achieved in ionic liquid (ILs) electrolytes composed of aluminum chloride ($AlCl_3$) and organic salts such as 1-butylpyridinium chloride, 1-ethyl-3-methylimidazolium chloride, and 1-butyl-3-methylimidazolium chloride ([BMIm]Cl).[5−7] Utilizing IL electrolytes, aluminum−chlorine (Al−Cl_2) rechargeable batteries were demonstrated by Gifford and Palmisano.[8] Despite the high discharge voltage (>1.5 V), good capacity, and cycle stability, the gaseous Cl_2 cathode was problematic. Furthermore, the Cl_2 cathode had to be first generated from the electrolysis of electrolyte through charging, which was also undesirable. More recently, vanadium oxide,[9,10] fluorinated graphite,[11] chloroaluminate-doped conductive polymers,[12] and graphitic carbons[13] were also reported as cathode materials vs Al in the IL-based electrolytes.

Unlike lithium, electrochemical Al intercalation into a host crystal structure can be very difficult due to the strong Coulombic effect induced by the three positive charges carried by the Al cation. Therefore, transition metal oxides, i.e., oxide anionic frameworks, may not be the ideal hosts for Al because of their strong electrostatic attraction with Al cations. It can hinder the redistribution of the charge of Al cations in the crystal, thus preventing the Al intercalation. On the other hand, sulfur has lower electronegativity than oxygen and is more polarizable due to its larger atom radius. Therefore, the charge redistribution in the sulfide anionic frameworks should be superior to oxides. Based on this concept, we demonstrate in this study the reversible electrochemical Al intercalation in Chevrel phase molybdenum sulfide (Mo_6S_8) for the first time.

Mo_6S_8 has a unique crystal structure of stacked Mo_6S_8 blocks composed of an octahedral cluster of Mo atoms inside a sulfur anion cubic cell. It is known to have two types of sites between the sulfur cubes that are capable to accommodate small cations such as Li^+, Cu^+, and Mg^{2+}.[14,15] Aurbach and co-workers first demonstrated Mo_6S_8 as a cathode material for rechargeable magnesium-ion batteries.[16] In this study, we synthesized Mo_6S_8 particles through a precipitation method modified from the reported works by Kumta et al.[17] and Liu et al.[18] As shown in the scanning electron microscopy (SEM) image in Figure 1a,

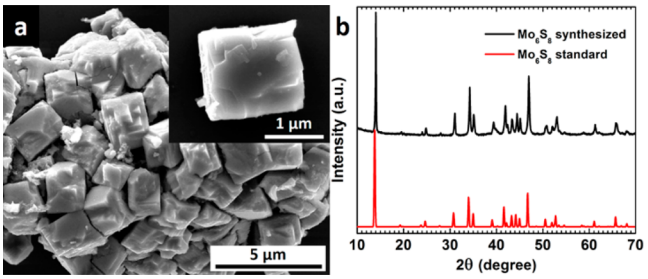

Figure 1. (a) SEM image and (b) XRD pattern of the synthesized Mo_6S_8.

the particle shape is cubic and the typical particle size is within the range of 1−2 μm. Figure 1b shows the X-ray powder diffraction (XRD) pattern, which is in excellent agreement with the pure Mo_6S_8 standard without the typical impurity of MoS_2.

The electrochemical Al intercalation in Mo_6S_8 was analyzed in CR2016 coin cells with Al foil as the counter/reference electrode. An IL electrolyte composed of a mixture of $AlCl_3$ and [BMIm]Cl with a molar ratio of 1.5:1 was used. It has been demonstrated that reversible Al deposition−dissolution can only be achieved in a Lewis acidic electrolyte composed of $AlCl_3$ and an IL with molar ratio > 1, and the electroactive species in the electrolyte is $[Al_2Cl_7]^-$ anion.[19] Indeed, facile Al deposition−dissolution was enabled by the prepared $AlCl_3$-[BMIm]Cl electrolyte as shown in Figure S1 in the Supporting Information. The results of the electrochemical characterizations of Mo_6S_8 vs Al are presented in Figure 2. Cyclic voltammetry (CV, scan rate =0.1 mV s^{-1}) were first performed at both room temperature (Figure S2 in the Supporting Information) and 50 °C. The electrochemical characteristics at these two temperatures are essentially the same; however, the elevated temperature apparently improved the electrochemical reaction kinetics indicated by the distinct shape of the current peaks and the narrowed redox peak separation as shown in Figure 2a. Therefore, the presented electrochemical studies were all performed at 50 °C. The room temperature electrochemical characterizations are shown as a comparison in the Supporting Information. It is worth noting that the ionic

Received: May 21, 2015
Revised: July 1, 2015
Published: July 6, 2015

DOI: 10.1021/acs.chemmater.5b01918
Chem. Mater. 2015, 27, 4926−4929

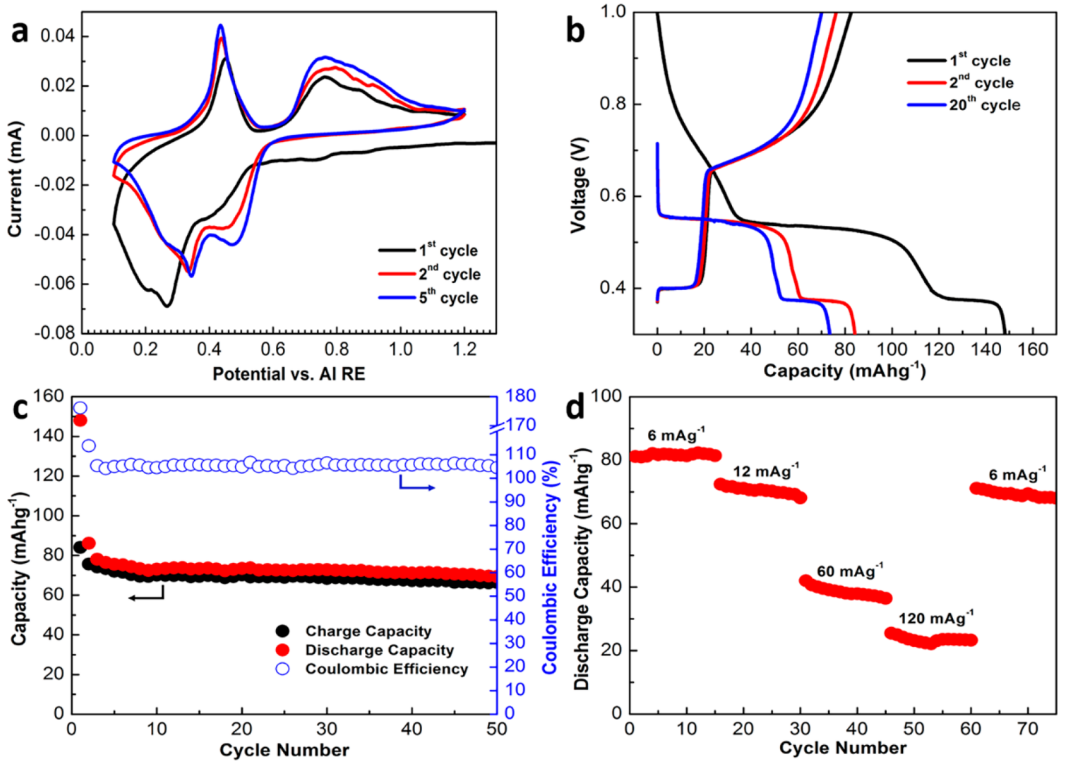

Figure 2. Electrochemical characterizations of Al-Mo_6S_8 cells at 50 °C. (a) The 1st, 2nd, and 5th CV curves of Mo_6S_8. (b) 1st, 2nd, and 20th GCD curves of Mo_6S_8 electrode vs Al. (c) Cycle stability and (d) rate capability of Al-Mo_6S_8 cells.

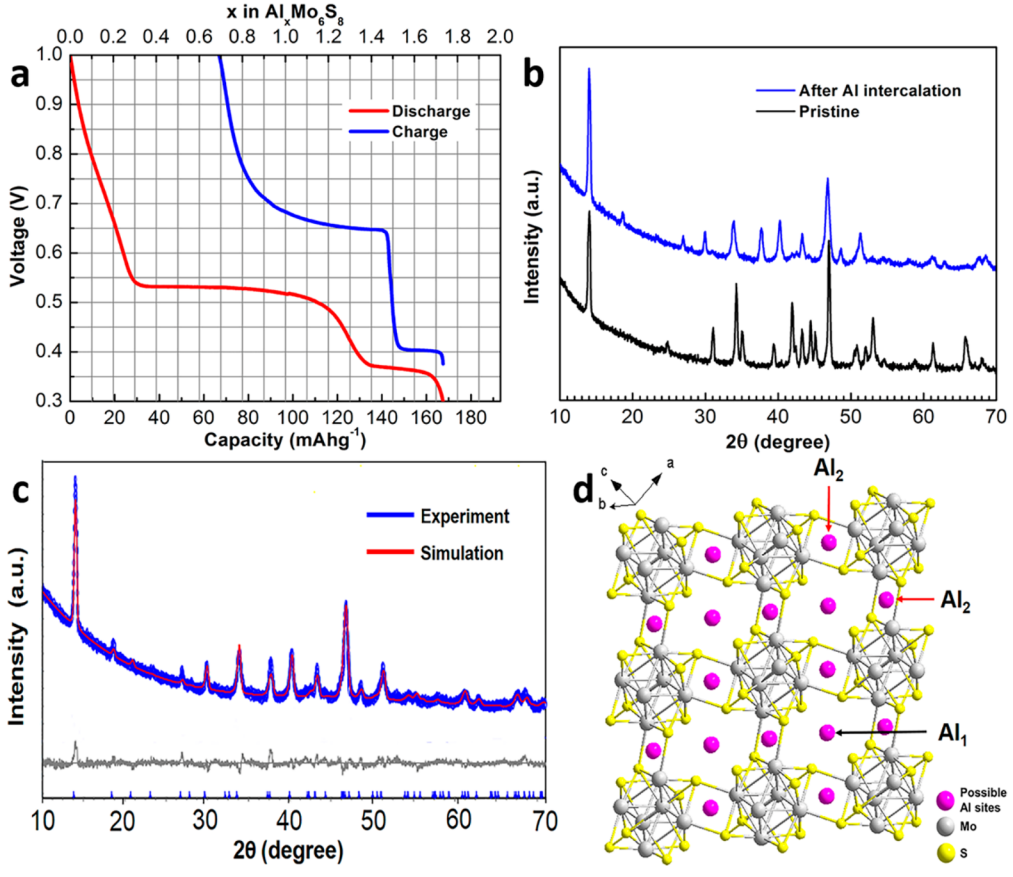

Figure 3. (a) Composition of Al intercalated Mo_6S_8 vs capacity. (b) XRD, (c) Rietveld refinement, and (d) crystal structure of Al intercalated Mo_6S_8.

DOI: 10.1021/acs.chemmater.5b01918
Chem. Mater. 2015, 27, 4926−4929

conductivity of the $AlCl_3$-[BMIm]Cl electrolyte is 2.21×10^{-2} S cm^{-1} at room temperature and 3.29×10^{-2} S cm^{-1} at 50 °C, both of which are sufficient for facile ion conducting. Therefore, the sluggish kinetics at room temperature may not be due to the low conductivity of the electrolyte but to the large particle size of Mo_6S_8, i.e., long solid-state diffusion pathway of Al.

As shown in Figure 2a, the stabilized CV scans of Mo_6S_8 vs Al demonstrate two cathodic peaks at 0.50 and 0.36 V and two corresponding anodic peaks at 0.40 and 0.75 V, indicating a two-step electrochemical reaction between Mo_6S_8 and Al. We speculate that these two pairs of CV peaks represent the Al intercalation/extraction in/from the two different sites in Mo_6S_8, which is verified by the crystallographic study described in the later section. A small additional cathodic peak at 0.20 V in the first scan and 0.26 V in the following scans, respectively, is also observed. This peak may be due to certain irreversible decomposition of the electrolyte, which is under investigation. Figure 2b depicts the representative galvanostatic charge−discharge (GCD) curves of the Al−Mo_6S_8 coin cell with a current density of 12 mA g^{-1} at 50 °C at the 1st, 2nd, and 20th cycles. The first discharge curve demonstrates two distinct plateaus at 0.55 and 0.37 V, which are consistent with the two cathodic peaks in the CV. These two discharge plateaus also indicate two phase-transition processes induced by the Al intercalation. The Al intercalation capacity in the first discharge is 148 mA h g^{-1} (based on the chemical formula weight of Mo_6S_8). However, the first charging capacity is only 85 mA h g^{-1}. By comparing the length of the discharge plateaus with the corresponding charged ones, it is clear that the intercalated Al atoms are partially trapped in the Mo_6S_8 crystal lattice. Furthermore, the voltage slope from 0.75 to 0.55 V in the first discharge curve, which may be due to the solid-solution Al intercalation prior to phase-transition, is significantly reduced in the subsequent discharges, which also contributes to the irreversible capacity. We attribute the irreversible capacity to the electrostatic attraction between Al cations and the sulfide anionic framework.[20] Nevertheless, the Mo_6S_8 electrode exhibits promising cycle stability: as shown in Figure 2c, the discharge capacity of Mo_6S_8 is quickly stabilized after the first cycle and retains a capacity of 70 mA h g^{-1} after 50 cycles. After cycling, the morphology of the Mo_6S_8 particles was analyzed with SEM. As shown in Figure S3 in the Supporting Information, cracks on the cycled Mo_6S_8 particles are visible, which suggests the large mechanical stress imposed by the Al intercalation. Therefore, the physical degradation of the Mo_6S_8 particles during cycling may be one of the reasons for the slow capacity fading. Another reason may still be the gradual Al trapping in Mo_6S_8 crystal, which is suggested by the >100% Coulombic efficiency (intercalation/extraction > 1). The Al−Mo_6S_8 coin cells were also discharged/charged at different current densities from 6 mA g^{-1} to 120 mA g^{-1}. As shown in Figure 2d, the Mo_6S_8 electrode can deliver a discharge capacity of 40 mA h g^{-1} and 25 mA h g^{-1} at current densities of 60 mA g^{-1} and 120 mA g^{-1}, respectively. In addition, the discharge capacity can be recovered to 70 mA h g^{-1} after changing the current density from 120 mA g^{-1} back to 6 mA g^{-1}. The Al−Mo_6S_8 intercalation behaviors in electrolytes with different $AlCl_3$/[BMIm]Cl ratio (acidity) are shown in Figure S4 in the Supporting Information.

To further analyze the composition and the crystal structure of the Al intercalated Mo_6S_8 ($Al_xMo_6S_8$), discharge−charge chronopotentiometry was performed using a small current density of 2.4 mA g^{-1}. As shown in Figure 3a, the electrochemically achievable Al interaction capacity is 167 mA h g^{-1}, which is equivalent to a formula of $Al_{1.73}Mo_6S_8$. The Al intercalated Mo_6S_8 sample was subsequently analyzed with the inductively coupled plasma optical emission spectrometry (ICP-OES) to verify the Al content. The ICP-OES result (Figure S5 in the Supporting Information) demonstrates that the chemical composition of the Al intercalated Mo_6S_8 is $Al_{1.67}Mo_6S_8$, which is in great agreement with the composition obtained from the chronopotentiometry experiment. Meanwhile, the charge curve in Figure 3a confirms that part of the Al atoms is trapped resulting in a chemical formula of $Al_{0.69}Mo_6S_8$ after Al extraction.

The XRD pattern of the Al intercalated Mo_6S_8 from the chronopotentiometry described above is shown in Figure 3b, which is distinctly different from that of the pristine Mo_6S_8. Rietveld refinement (TOPAS program) was performed to obtain the crystal structure parameters of the Al intercalated Mo_6S_8. Chevrel phase $Ga_2Mo_6S_8$ was used as the starting structural model.[21] As shown in Figure 3c, the refinement XRD pattern (red line) is in excellent agreement with the experimental data (blue line). The Rietveld refinement results including various agreement factors are listed in Table 1. The

Table 1. Lattice Parameters of $Al_2Mo_6S_8$

space group: $R\bar{3}H$	R_{exp}: 2.37
a (Å): 9.6356	R_{wp}: 4.58
c (Å): 9.9942	R_p: 3.40
cell volume (Å^3): 803.5904	R-Bragg: 3.312
crystallite size (nm): 145.2	GOF: 1.93

refinement result supports the hypothesis that Al atoms are intercalated into two different sites in the Mo_6S_8 lattice with a theoretical formula of $Al_2Mo_6S_8$ at full Al intercalation (theoretical capacity of 193 mA h g^{-1}). The crystal structure of $Al_2Mo_6S_8$ is illustrated in Figure 3d, showing the packing of Mo_6S_8 units and Al atoms intercalated in two different sites. The larger site (Al_1) can be seen as a cubic center of a hexahedron with eight Mo_6S_8 units as the vertices, while the smaller site (Al_2) can be seen as face centered. Crystallographic views of $Al_2Mo_6S_8$ from more directions are shown in Figure S6 in the Supporting Information. Al can be more easily intercalated into the Al_1 sites leading to a stoichiometric formula of $AlMo_6S_8$ (corresponding to the first discharge plateau). As for the Al_2 sites, although we can identify six available sites on the faces of the hexahedron mentioned above, the strong electrostatic force from the Al cation with three positive charges can only allow filling in two of the six sites,[21] which also gives a stoichiometric formula of $AlMo_6S_8$ (corresponding to the second discharge plateau). Therefore, the fully Al intercalated formula is $Al_2Mo_6S_8$, which is consistent with the refinement result. The discharge and charge reactions are proposed as follows:

$$Al + 7[AlCl_4]^- \leftrightarrow 4[Al_2Cl_7]^- + 3e^- \quad \text{(anode)}$$

$$8[Al_2Cl_7]^- + 6e^- + Mo_6S_8 \leftrightarrow Al_2Mo_6S_8 + 14[AlCl_4]^- \quad \text{(cathode)}$$

In conclusion, Mo_6S_8 shows unambiguous electrochemical activity for reversible Al intercalation and extraction with good cycle stability. In addition to the electrochemical analysis, XRD investigations provide the crystallographic information on the

DOI: 10.1021/acs.chemmater.5b01918
Chem. Mater. 2015, 27, 4926−4929

Al intercalated Mo_6S_8. We conclude that the theoretical formula of fully Al intercalated Mo_6S_8 is $Al_2Mo_6S_8$ with Al occupying two different sites in the Mo_6S_8 crystal lattice. From the practical aspect, the theoretical material-level specific energy of a battery with Al anode and Mo_6S_8 cathode is approximately 90 W h kg^{-1} (assuming 0.5 V nominal voltage), which can be an attractive alternative for large-scale energy storage technologies. Further investigation is under way to understand the Al trapping mechanism and to address the large irreversible capacity in the first cycle.

■ ASSOCIATED CONTENT

Supporting Information

Experimental details, Al deposition−dissolution, additional electrochemical characterizations, elemental analysis result of Mo_6S_8 after Al intercalation, crystallographic views from different directions, and SEM images of Mo_6S_8 after cycling. The Supporting Information is available free of charge on the ACS Publications website at DOI: 10.1021/acs.chemmater.5b01918.

■ AUTHOR INFORMATION

Corresponding Author

*E-mail: jguo@engr.ucr.edu.

Notes

The authors declare no competing financial interest.

■ ACKNOWLEDGMENTS

This work is supported by the University of California, Riverside, and the Hellman Fellowship. G.Lv acknowledges the support from China Scholarship Council. The authors also thank Mr. Xitong Chen from Prof. Pingyun Feng's group in the Chemistry Department at UCR for the helpful discussion.

■ REFERENCES

(1) Li, Q.; Bjerrum, N. J. Aluminum as anode for energy storage and conversion: a review. *J. Power Sources* **2002**, *110*, 1.

(2) Matsuda, Y.; Ouchi, Y.; Tamura, H. Anodic polarization of aluminum in organic electrolytes. *J. Appl. Electrochem.* **1974**, *4*, 53.

(3) Licht, S.; Levitin, G.; Yarnitzky, C.; Tel-Vered, R. The Organic Phase for Aluminum Batteries. *Electrochem. Solid-State Lett.* **1999**, *2*, 262.

(4) Levitin, G.; Yarnitzky, C.; Licht, S. Fluorinated Graphites as Energetic Cathodes for Nonaqueous Al Batteries. *Electrochem. Solid-State Lett.* **2002**, *5*, A160.

(5) Endres, F. Ionic Liquids: Solvents for the Electrodeposition of Metals and Semiconductors. *ChemPhysChem* **2002**, *3*, 144.

(6) Jiang, T.; Chollier Brym, M. J.; Dube, G.; Lasia, A.; Brisard, G. M. Electrodeposition of aluminium from ionic liquids: Part I—electrodeposition and surface morphology of aluminium from aluminium chloride (AlCl3)−1-ethyl-3 methylimidazolium chloride ([EMIm]Cl) ionic liquids. *Surf. Coat. Technol.* **2006**, *201*, 1.

(7) Jiang, T.; Chollier Brym, M. J.; Dube, G.; Lasia, A.; Brisard, G. M. Electrodeposition of aluminium from ionic liquids: Part II - studies on the electrodeposition of aluminum from aluminum chloride (AlCl3) - trimethylphenylammonium chloride (TMPAC) ionic liquids. *Surf. Coat. Technol.* **2006**, *201*, 10.

(8) Gifford, P. R.; Palmisano, J. B. An Aluminum/Chlorine Rechargeable Cell Employing a Room Temperature Molten Salt Electrolyte. *J. Electrochem. Soc.* **1988**, *135*, 650−654.

(9) Jayaprakash, N.; Das, S. K.; Archer, L. A. The rechargeable aluminum-ion battery. *Chem. Commun.* **2011**, *47*, 12610.

(10) Reed, L. D.; Menke, E. The Roles of V2O5 and Stainless Steel in Rechargeable Al−Ion Batteries. *J. Electrochem. Soc.* **2013**, *160*, A915.

(11) Rani, J. V.; Kanakaiah, V.; Dadmal, T.; Srinivasa Rao, M.; Bhavanarushi, S. Fluorinated Natural Graphite Cathode for Rechargeable Ionic Liquid Based Aluminum−Ion Battery. *J. Electrochem. Soc.* **2013**, *160*, A1781.

(12) Hudak, N. S. Chloroaluminate-doped conducting polymers as positive electrodes in rechargeable aluminum batteries. *J. Phys. Chem. C* **2014**, *118*, 5203.

(13) Lin, M.; Gong, M.; Lu, B.; Wu, Y.; Wang, D.; Guan, M.; Angell, M.; Chen, C.; Yang, J.; Hwang, B.; Dai, H. An ultrafast rechargeable aluminium-ion battery. *Nature* **2015**, *520*, 324−328.

(14) Ritter, C.; Gocke, E.; Fischer, C.; Schollhorn, R. Neutron diffraction study of the crystal structure of lithium intercalated Chevrel phases. *Mater. Res. Bull.* **1992**, *27*, 1217.

(15) Levi, E.; Lancry, E.; Mitelman, A.; Aurbach, D.; Ceder, G.; Morgan, D.; Isnard, O. Phase Diagram of Mg Insertion into Chevrel Phases, $Mg_xMo_6T_8$ (T = S, Se). 1. Crystal Structure of the Sulfides. *Chem. Mater.* **2006**, *18*, 5492.

(16) Aurbach, D.; Lu, Z.; Schechter, A.; Gofer, Y.; Gizbar, H.; Turgeman, R.; Cohen, Y.; Moshkovich, M.; Levi, E. Prototype systems for rechargeable magnesium batteries. *Nature* **2000**, *407*, 724.

(17) Saha, P.; Jampani, P. H.; Datta, M. K.; Okoli, C. U.; Manivannan, A.; Kumta, P. N. A Convenient Approach to Mo_6S_8 Chevrel Phase Cathode for Rechargeable Magnesium Battery. *J. Electrochem. Soc.* **2014**, *161*, A593.

(18) Cheng, Y.; Parent, L. R.; Shao, Y.; Wang, C.; Sprenkle, V. L.; Li, G.; Liu, J. Facile Synthesis of Chevrel Phase Nanocubes and Their Applications for Multivalent Energy Storage. *Chem. Mater.* **2014**, *26*, 4904.

(19) Stark, J. K.; Ding, Y.; Kohl, P. A. Dendrite-Free Electrodeposition and Reoxidation of Lithium-Sodium Alloy for Metal-Anode Battery. *J. Electrochem. Soc.* **2011**, *158*, A1100.

(20) Mitelman, A.; Levi, E.; Lancry, E.; Aurbach, D. On the Mg Trapping Mechanism in Electrodes Comprising Chevrel Phases. *ECS Trans* **2007**, *3*, 109.

(21) Schmidt, A. M. Investigation of New Chevrel Phase Compounds for Improved Efficiency of Thermoelectric Power Generation Devices. M.S. Thesis, Cornell University, August, 2005.

DOI: 10.1021/acs.chemmater.5b01918
Chem. Mater. 2015, 27, 4926−4929

Supporting Information

Reversible Electrochemical Intercalation of Aluminum in Mo_6S_8

Linxiao Geng,[†] Guocheng Lv,[§] Xuebing Xing,[§] Juchen Guo [,†,‡]*

[†] Department of Chemical and Environmental Engineering, University of California, Riverside, Riverside, CA 92521, USA
[‡] Materials Science and Engineering Program, University of California, Riverside, Riverside, CA 92521, USA
[§] School of Materials Sciences and Technology, China University of Geosciences, Beijing, Beijing, 100083, China

Corresponding Author
* Email: jguo@engr.ucr.edu

EXPERIMENTAL

Synthesis of Chevrel Phase Mo_6S_8. All reagents were used after purchase without further purification unless otherwise noted. In a typical synthesis of Mo_6S_8, stoichiometric amounts of anhydrous copper(II) chloride ($CuCl_2$, 0.3442 g, 2.56 mmol, Sigma Aldrich 99.995%) and ammonium tetrathiomolybdate ($(NH_4)_2MoS_4$, 2.000 g, 7.68 mmol; Fisher Scientific 99.99%) were dissolved in 65 mL N,N-Dimethylformamide (DMF, Sigma Aldrich 99.8%) and the mixture was stirred for 30 min at room temperature. The resultant solution was then heated at 90 °C for 6 hours under continuous argon bubbling. After the reaction was completed, the solution was filtered, and then 325 mL THF (1:5 by volume) was added immediately to the filtrate to initiate precipitation. The precipitate was collected by centrifuge, washed with THF and dried in the vacuum oven at 150 °C overnight. The dried solid agglomerate was then ground and heated in a tube furnace at 1000 °C for 7 hour under reducing environment (95 vol.% argon and 5 vol.% H_2) to yield Chevrel phase $Cu_2Mo_6S_8$. The obtained $Cu_2Mo_6S_8$ was then added into 20 mL 6M HCl solution. Oxygen was bubbled into the solution for 8 hours while stirring to leach out Cu to yield Mo_6S_8. After the reaction, the obtained Mo_6S_8 was centrifuged, washed with adequate amount of deionized water, and dried in vacuum oven at 50 °C overnight.

Electrochemical Analysis. For battery preparation, Al foil with 0.2 mm thickness (Alfa Aesar 99.9999%) was used as the anode. Cathode was fabricated by coating Mo_6S_8 slurry onto carbon paper current collector (Fuel Cell Earth). The carbon paper current collector was demonstrated to be electrochemically inert in the applied potential window as shown in Figure S7. The slurry was made by mixing 80 wt.% Mo_6S_8, 10 wt.% carbon black, and 10 wt.% polyvinylidene fluoride in N-Methyl-2-pyrrolidone solution via a mechanical mixer for 5 min in an argon-filled glovebox. A single Whitman® glass fiber filter was used as the separator. The electrolyte was synthesized by slowly adding anhydrous $AlCl_3$ (Sigma Aldrich 99.99%) into [BMIm]Cl (Sigma Aldrich 99.0%) with a molar ratio of 1.5:1 while stirring. Both $AlCl_3$ and [BMIm]Cl were further dried in vacuum oven at 150 °C overnight prior mixing. CR2016 coin cells were assembled in the argon-filled glovebox. To prevent potential corrosion from the acidic electrolyte, titanium foil was used as lining at both electrodes inside the stainless steel coin cell case.

The cyclic voltammetry (CV) of Al deposition-dissolution and the galvanostatic Al deposition were performed in three-electrode cells with a Gamry potentiostat/galvanostat/ZRA (Interface 3000) using Nickel (0.025 mm thick, Alfa Aesar 99.5%) working electrode and two Al wires (2.0 mm diameter, Alfa Aesar 99.9995%) as the counter and the reference electrodes, respectively. The CV scan rate for Al deposition-dissolution experiment was 100 mV s^{-1} from -1.0 V to 2.0 V vs. Al. A constant current density of -5 mA cm^{-2} was applied in electrochemical Al deposition experiment. The ionic conductivity of the $AlCl_3$-[BMIm]Cl electrolyte at room temperature and 50 °C was obtained from the resistance measurement in a cell with two parallel Pt electrodes. The cell constant was obtained through calibration using standard aqueous KCl solutions. The resistance was measured with a Gamry potentiostat/galvanostat/ZRA (Interface 1000). The GCD experiments of Al-Mo_6S_8 batteries were performed on an Arbin battery test station, and the CV analysis of Al-Mo_6S_8 was conducted on a Gamry Interface 1000 with a scan rate of 0.1 mV s^{-1}.

Materials Characterization. The surface area of the synthesized Mo_6S_8 was measured with nitrogen adsorption-desorption method, and the isotherms are shown in Figure S8. The BET surface area of the Mo_6S_8 is 6.9 m^2 g^{-1}. The X-ray diffraction (XRD) was conducted using PANalytical EMPYREAN instrument (45 kV/40 mA) with a Cu-Kα source. The inductively coupled plasma optical emission spectrometry (ICP-OES) of Al intercalated Mo_6S_8 was performed by Elemental Analysis, Inc. (Lexington, KY). Prior to the ICP-OES analysis, the Al-Mo_6S_8 coin cell was dissembled in the argon-filled glovebox. The electrode containing Mo_6S_8 particles was first soaked in 3 ml NMP and sonicated for 5 minutes. The NMP dissolved the PVDF polymer binder and suspended the powder (Mo_6S_8 and carbon black) in the solution. The suspension was centrifuged and the collected powder was further washed three times with NMP followed by adequate THF for three times to remove the electrolyte residue. Finally, the powder was vacuum dried at 60 °C overnight. The Rietveld refinement was performed using the TOPAS program. Scanning electron microscopy (SEM) was performed with a FEI XL30-FEG (10 kV/192 μA).

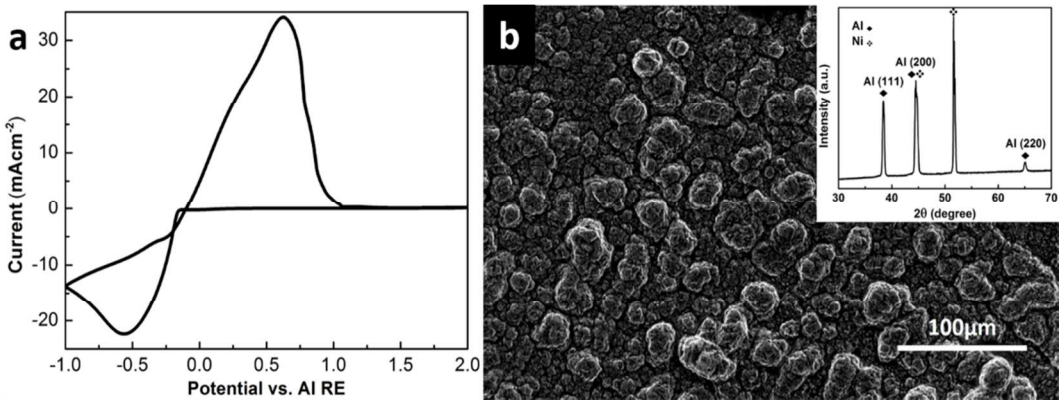

Figure S1. (a) The CV scan of Al deposition-dissolution on Ni working electrode in the $AlCl_3$-[BMIm]Cl electrolyte ($AlCl_3$:[BMIm]Cl = 1.5:1). The CV curves demonstrate facile Al deposition-dissolution with small deposition overpotential of 200 mV; (b) the SEM image of the deposited Al on Ni, inset shows the XRD of the deposited Al.

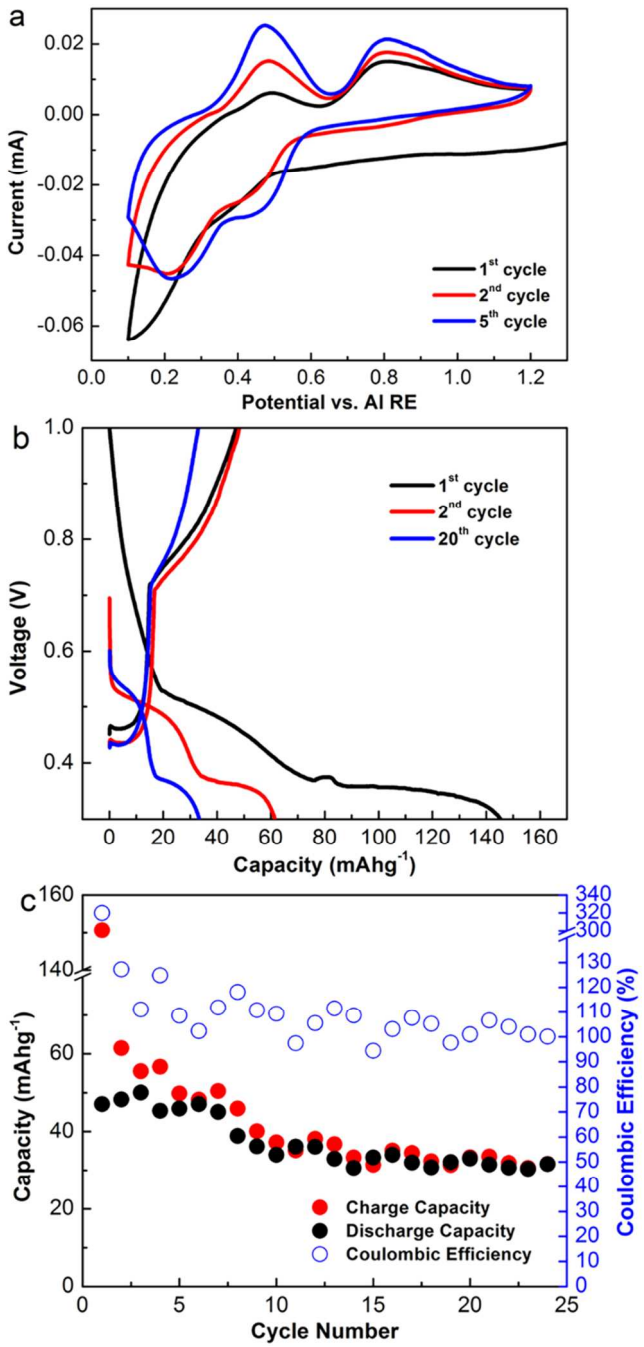

Figure S2. Electrochemical characterization of the Al-Mo_6S_8 cells at room temperature: (a) The 1st, 2nd and 5th CV curves of Mo_6S_8 vs. Al with a scan rate of 0.1 mV s^{-1} in the range of 0.1 V to 1.2 V. (b) First two GCD curves of Al-Mo_6S_8 cell with a current density of 12 mA g^{-1} in the voltage window of 0.3 V to 1.0 V. (c) Cycle stability of first 24 cycles at room temperature with discharge/charge rate of 12 mA g^{-1}.

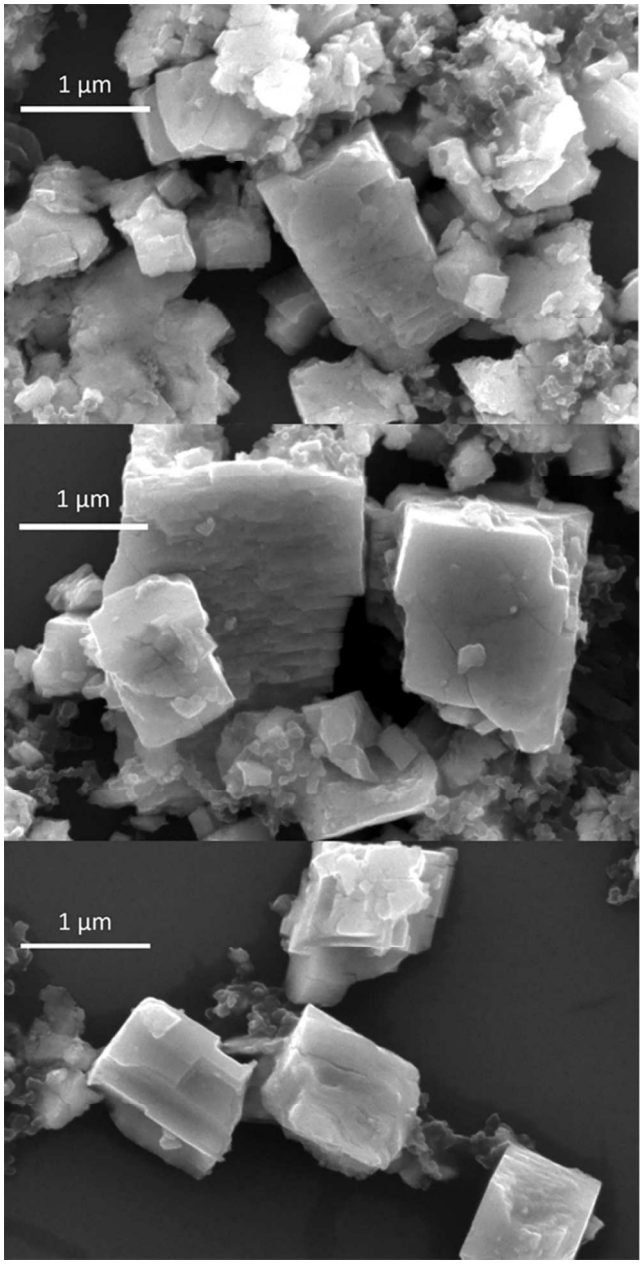

Figure S3. SEM images of the Chevrel phase Mo_6S_8 after 50 cycles of galvanostatic charge-discharge with a current density of 12 mA g^{-1}.

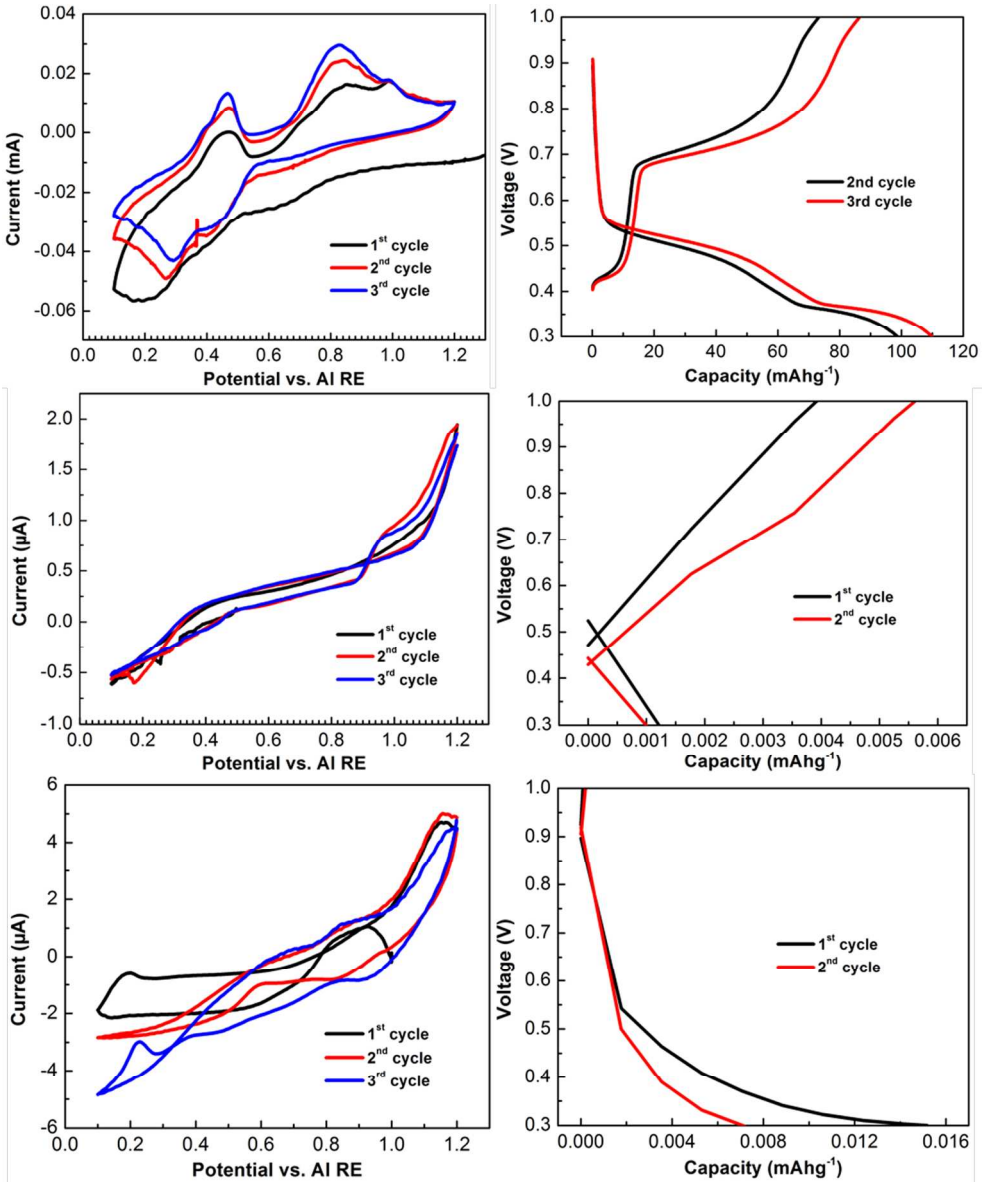

Figure S4. Electrochemical behaviors of Al-Mo_6S_8 in electrolytes with different $AlCl_3$/[BMIm]Cl ratio at 50°C: $AlCl_3$:[BMIm]Cl=1.1:1 (top), $AlCl_3$:[BMIm]Cl=1:1 (middle) and $AlCl_3$:[BMIm]Cl=0.9:1 (bottom). The CV scan rate is 0.1 mV s^{-1} and the GCD current density is 12 mA g^{-1}. Comparing with the electrolyte ($AlCl_3$:[BMIm]Cl = 1.5:1) used in the study, the electrolyte with $AlCl_3$:[BMIm]Cl = 1.1:1 is still Lewis acidic containing active species $[Al_2Cl_7]^-$. This acidic electrolyte is still able to enable the reversible Al intercalation-extraction as indicated by the CV and GCD curves. It is also noticed that the CV peak separation and charge-discharge hysteresis become larger, which can be attributed to the lower acidity (i.e. lower concentration of $[Al_2Cl_7]^-$). The electrolyte with $AlCl_3$:[BMIm]Cl = 1:1 is neutral without $[Al_2Cl_7]^-$ (species in the electrolyte are $[AlCl_4]^-$ and $[BMIm]^+$). It does not enable any electrochemical activity between Al and Mo_6S_8, noticing the current of the CV and the capacity demonstrated in the GCD are extremely low. The similar non-active behavior is also demonstrated by the Lewis base electrolyte ($AlCl_3$:[BMIm]Cl = 0.9:1).

EAI ~ Elemental Analysis, Inc.

Thursday, March 12, 2015

Dr. Juchen Guo,
University of California, Riverside
900 University Ave Bourns Hall A220
Riverside CA 92521

Phone: (951) 827-6472
Email: jguo@engr.ucr.edu

EAI Project: 1380-15

Aluminum and Molybdenum by Inductively Coupled Plasma Optical Emission Spectrometry

Sample ID	Aluminum (wt%)	Molybdenum (wt%)
#1	2.38%	30.35%

Respectfully Submitted,
Elemental Analysis Incorporated

Nick Tzouanakis,
Technical Sales Representative

2101 Capstone Drive, Suite 110, Lexington, KY 40511
Phone: 800-563-7493 / Fax: 859-254-5150 Email: Trace@ElementalAnalysis.com

Figure S5. Report of Al and Mo contents via ICP-OES from Elemental Analysis, Inc. The rest content in the sample includes sulfur, carbon black, and polymer binder residue.

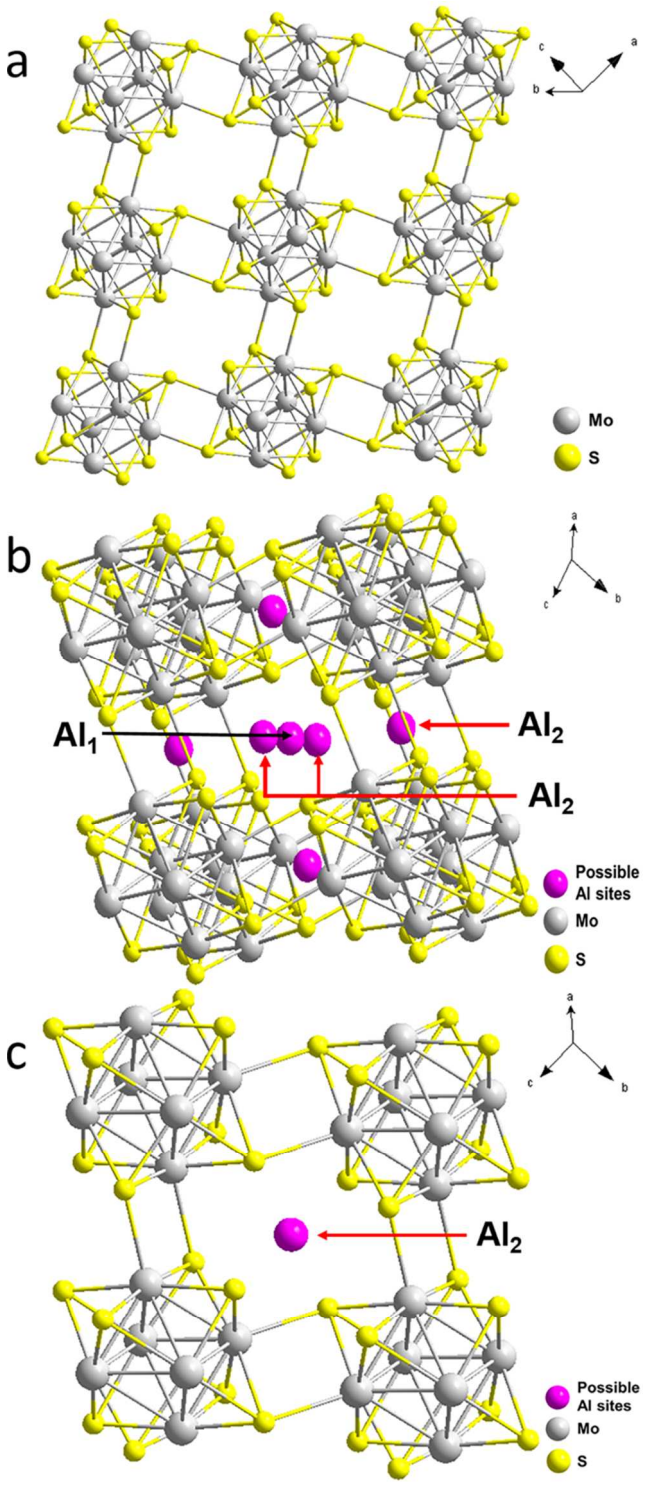

Figure S6. (a) Crystal structure of the pristine Chevrel phase Mo_6S_8. (b) Schematic of Chevrel phase Mo_6S_8 and possible Al intercalation sites. (c) Schematic of the smaller Al intercalation site (inner site) which can be interpreted as in the center of the square with four Mo_6S_8 clusters as vertices.

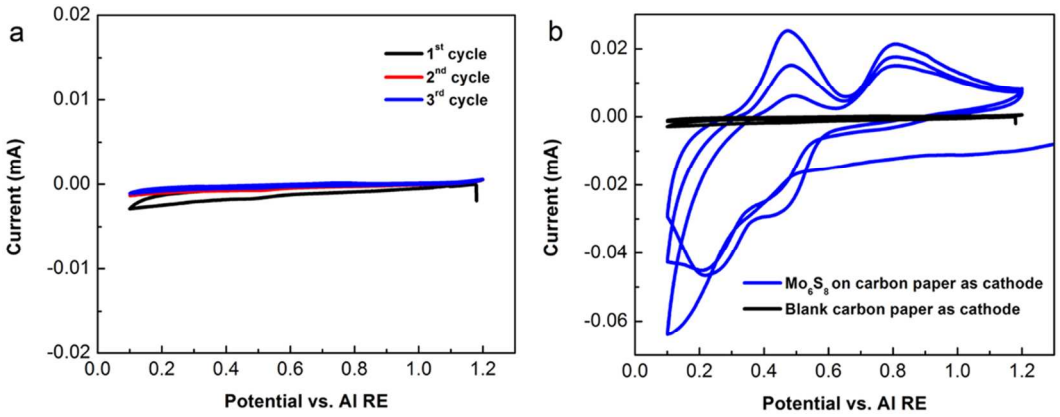

Figure S7. (a) Electrochemical stability test of the carbon paper current collector via CV (0.1 mV s^{-1}, Al RE and Al CE) at room temperature. The scan rate and experiment set up are the same as when using Mo_6S_8 cathode. (b) Comparison between CV curves of Mo_6S_8 on carbon paper vs. Al and blank carbon paper vs. Al at room temperature. These plots clearly demonstrated the electrochemical stability of the carbon paper current collector.

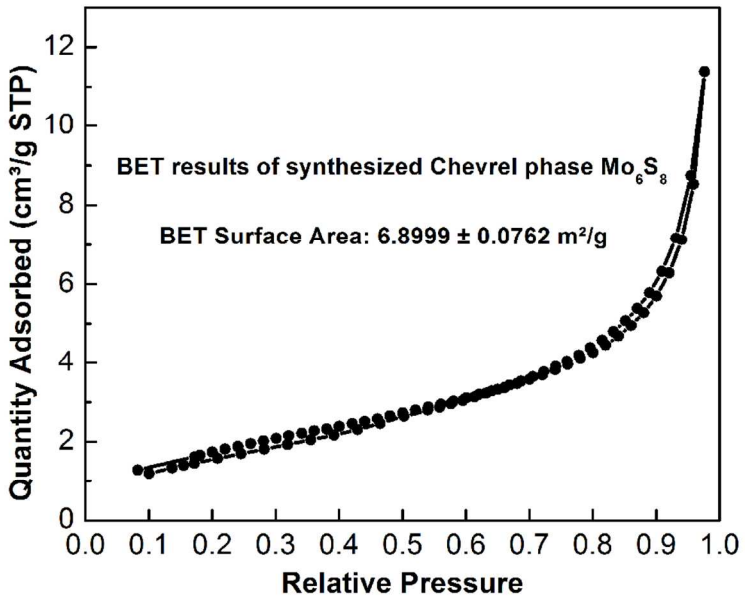

Figure S8. N_2 adsorption-desorption isotherms of the synthesized Mo_6S_8 powder.